Journal of Applied Mechanics Vol.8, pp.565-571 (August 2005) JSCE

Non-coaxial constitutive response of idealized 3D granular assemblies to rotation of principal stress axes

Seiichiro Tsutsumi*, Kenji Kaneko**, Masahiro Toyosada**, Koichi Hashiguchi****, Yuji Kishino*****

* Dr. of Agr., Research Associate, Dept. of Marine System Eng., Kyushu University, Fukuoka 812-8581
** Dr. of Eng., Assistant Professor, Dept. of Environmental and Civil Eng., Hachinohe Inst. Tech.,
*** Dr. of Eng., Professor, Dept. of Marine System Eng., Kyushu University, Fukuoka 812-8581
**** Dr. of Eng. and Dr. of Agr., Professor, Dept. of Agr. Eng., Kyushu University, Fukuoka 812-8581
***** Dr. of Eng., Professor, Dept. of Civil. Eng., Tohoku University, Sendai 980-8579

A method of multiscale analysis based on mathematical homogenization theory has been developed for quasi-static equilibrium problems of granular media. The micro-scale problem is analyzed by a discrete numerical model assuming elastic and frictional contact between rigid particles. This two-scale analysis enables us to obtain the macroscopic/phenomenological inelastic deformation response of a representative volume element (RVE). To examine the macroscopic deformation properties of the assumed RVE, a series of numerical experiments involving pure rotation of the principal stress axes are carried out. The necessity of incorporating the non-coaxiality induced by the tangent effect and the anisotropy in the yield condition is revealed in the phenomenological constitutive description of the deformation under principal stress axes rotation.

Key Words: granular element model, constitutive response, non-coaxiality

1. Introduction

The stress path often deviates severely from proportional loading in many real situations. The following results have been found experimentally for the non-proportional loading behavior of soils[1)-3)]: i) Not only the magnitude but also the direction of inelastic stretching is dependent on the direction of the stress rate, as revealed by stress probe tests, ii) Inelastic deformation is induced by the rotation of the principal stress axes, even if all of the values of the principal stresses and invariants of stress are kept constant. However, the physical tests have difficulty to derive absolute conclusions due to the restrictions of the test system and the variation of specimen.

On the other hand, numerical tests do not have these problems, because any intermediate data can be used for different tests and any stress or strain control can be applied flexibly. There have been many studies referring to numerical solutions, which can be obtained by discrete numerical models. The distinct element method (DEM)[4)] is one of the most popular discrete models. The DEM can be utilized to characterize the macroscopic elastic–plastic mechanical behavior of a granular assembly, but is suited mainly to dynamic motions.

For the quasi-static equilibrium states of granular media, Kishino (1989)[5), 6)] developed the granular element method (GEM) to study the flow rule and the stability conditions for granular media: see also Wren and Borja (1997)[7)] and Kuhn (1999)[8)] who utilized numerical methods similar to the GEM to study the macroscopic constitutive laws for granular media. Also, the entropy estimation of contact forces has been discussed[9)].

A method of multiscale analysis based on mathematical homogenization theory has been developed for quasi-static equilibrium problems of granular media by Kaneko (2001)[10)] and Kaneko et al. (2003)[11)]. The mathematical theory of homogenization for heterogeneous media with periodic microstructures enables us to realize the two-scale modeling, which consistently encompasses both micro- and macroscales together with variational statements. Due to this consistency, the nonlinear mechanical behavior is easily incorporated into the numerical analysis by the finite element method (FEM). The problem can be formulated in terms of two distinct scales; macro- and microscales. The former scale defines a global structure, the latter a local structure or equivalently a representative volume element (RVE). The macroscopic

field variables are simply calculated as the volume average of the corresponding microscopic variables over the RVE and satisfy quasi-static equilibrium of the overall structure. On the other hand, a particulate structure with friction-contact behavior is assigned to the RVE on the microscale. The RVE is assumed to be periodic throughout the paper and is often denoted as the unit cell. Then, the resulting two-scale boundary value problem allows us to analyze the microscale behavior of unit cells by the GEM, in which springs and friction sliders connect rigid particles, while the macroscopic problem is solved by the continuum-based FEM. The aforementioned experimental fact i) is verified by numerical experiments due to the GEM analysis for granular media[2), 3)].

In this study, the 3-dimensional two-scale modeling based on the mathematical homogenization method is adopted for the quasi-static numerical simulations of granular media in order to examine their mechanical response to pure rotation of the principal stress axes. Also, mechanical interpretation of the roles of the non-coaxiality for the description of the non-proportional loading behavior of materials are reviewed[12)-14)]. Then, based on this interpretation, the mechanical responses to the rotation of the principal stress axes are examined from the points of view of the both the tangent effect and the anisotropy in the yield condition, adopting the subloading surface model with the tangential effect and the anisotropic yield surface due to the rotation of the yield surface.

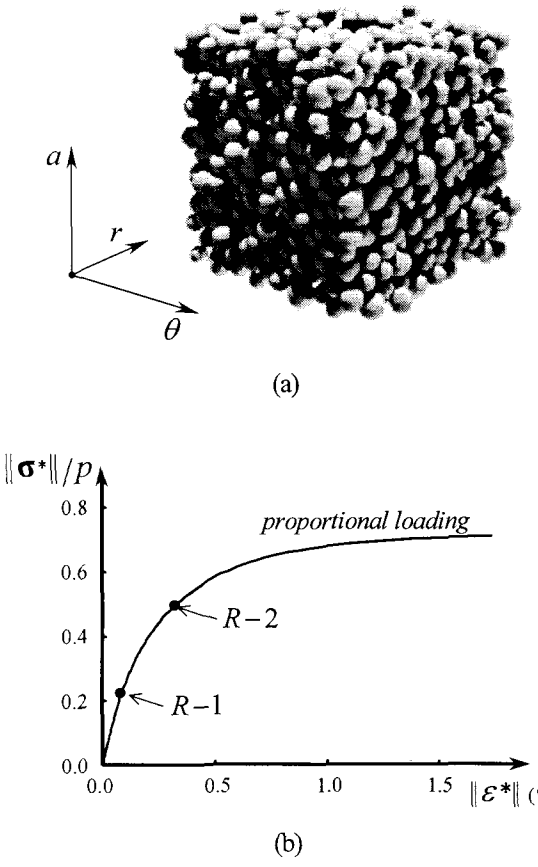

Figure 1 (a) Granular element model and (b) Stress-strain curve with the rotational path points R-1 and R-2.

2. Macroscopic constitutive responses predicted by granular element model

2.1 Granular assemblies

The body considered is a periodic assembly of micro-structural elements (RVE), in which the size of the RVE is small enough relative to the overall structure. In the two-scale method, the microscopic problem is treated numerically by means of the discrete Granular Element Method (GEM), while the macroscopic one is by a conventional finite element method.

The model under consideration, depicted in Figure 1(a), has 1776 spheres. After achieving the initial equilibrium state under confining pressure up to 100 kPa, tri-axial shear loading is applied under the stress-controlled and constant mean stress conditions, as has been done by some experiments[1)-3)]. The normal and tangential spring constants for the granular interaction are assumed to be 100 kPa and 70 kPa, respectively, while the friction angle is set to be tan(15°). Figure 1(b) shows the stress-strain relationship under monotonic triaxial compression condition. To examine the mechanical responses of the specimen to the non-proportional loading conditions, a series of tests are conducted from the loading points R-1 and R-2 shown in Figure 1(b). The specimen is subjected to principal stress axes rotation under the condition in which all of the invariants of stress are kept constant.

2.2 Test procedures

In the experiments using a hollow cylindrical specimen[1)-3)] the four stress components, i.e. the axial stress σ_a , the radial stress σ_r , the peripheral stress σ_θ and the torsional shear stress $\sigma_{a\theta}$, can be applied independently under the coordinate system (θ, r, a) . These four stress components are described by the effective pressure p, the magnitude $\| \ \|$ of the deviatoric stress $\boldsymbol{\sigma}^*$, the Lode's angle θ_σ and the rotation angle α of the principal stress axes as

$$\left.\begin{matrix}\sigma_\theta \\ \sigma_a\end{matrix}\right\} = -p + \sqrt{\frac{2}{3}}\,\|\boldsymbol{\sigma}^*\|\left(\frac{\sin\theta_\sigma}{3} \pm \frac{\cos\theta_\sigma \cos 2\alpha}{\sqrt{3}}\right) \tag{1}$$

$$\sigma_r = -p + \frac{2}{3}\sqrt{\frac{2}{3}}\,\|\boldsymbol{\sigma}^*\|\,\sin\theta_\sigma \tag{2}$$

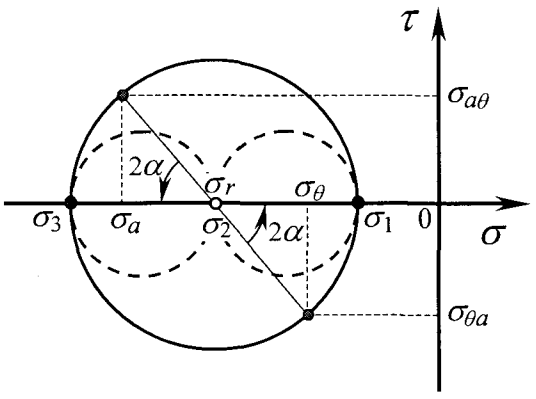

(a)

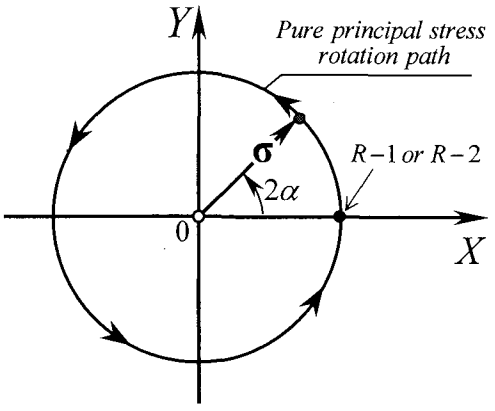

(b)

Figure 2 (a) Mohr's circle of stress and (b) the pure principal stress rotation path in (X, Y) plane.

$$\sigma_{a\theta} = \sqrt{\frac{2}{3}}\,\|\boldsymbol{\sigma}^*\|\,\frac{\cos\theta_\sigma \sin 2\alpha}{\sqrt{3}} \tag{3}$$

where

$$\theta_\sigma \equiv -\frac{1}{3}\sin^{-1}\left(\sqrt{6}\,\frac{\mathrm{tr}\boldsymbol{\sigma}^{*3}}{\|\boldsymbol{\sigma}^*\|^3}\right) = \tan^{-1}\frac{2\sigma_2-\sigma_1-\sigma_3}{\sqrt{3}(\sigma_1-\sigma_3)} \tag{4}$$

Equations (1)-(4) are derived by orthogonal transformation of the principal stresses to a coordinate system rotated around the intermediate principal stress axis ($\sigma_r = \sigma_2$). The b-value is related to Lode's angle as follows:

$$b \equiv \frac{\sigma_2-\sigma_3}{\sigma_1-\sigma_3} = \frac{1}{2}(\sqrt{3}\tan\theta_\sigma + 1) \tag{5}$$

In the tests adopted for later examination, however, the stresses are controlled to fulfill $\sigma_r = \sigma_2 = (\sigma_1+\sigma_3)/2$ = const., leading to $b = 0.5$, i.e. $\theta_\sigma = 0^\circ$. Then, Mohr's stress circle for the pure principal stress axes rotation is depicted as shown in Figure 2(a). The stress σ_θ, σ_r, σ_a and $\sigma_{a\theta}$ are described by the principal stresses and α as follows:

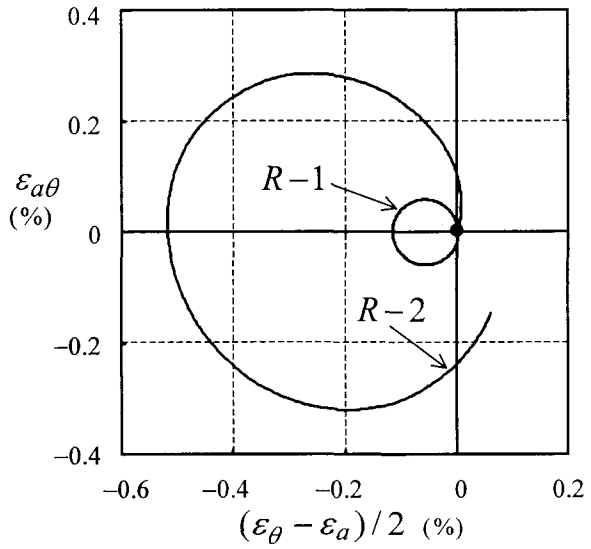

Figure 3 The inelastic strain in the principal stress rotation from the stress states R-1 and R-2.

$$\left.\begin{matrix}\sigma_\theta \\ \sigma_a\end{matrix}\right\} = \frac{\sigma_1+\sigma_3}{2} \pm \frac{\sigma_1-\sigma_3}{2}\cos 2\alpha,$$
$$\sigma_r = \sigma_2 = -p, \tag{6}$$
$$\sigma_{a\theta} = \frac{\sigma_1-\sigma_3}{2}\sin 2\alpha$$

The state of stress induced in the tests can also be represented in the (X, Y) stress plane (Fig. 2(b)), where

$$X = \frac{\sigma_\theta - \sigma_a}{2}, \quad Y = \sigma_{a\theta} \tag{7}$$

In the (X, Y) plane, the length of the stress vector is equal to the radius of Mohr's stress circle and makes twice the angle α, i.e.

$$\tan 2\alpha = \frac{Y}{X} \tag{8}$$

Strain increments induced by the imposed stress increments in the (X, Y) plane are also depicted taking $(d\varepsilon_\theta - d\varepsilon_a)/2$ and $d\varepsilon_{a\theta}$ for the X- and the Y-axis, respectively.

2.3 Rotation of principal stress axes of idealized granular assemblies

In the non-proportional loading calculation with a pure rotation of the principal stress axes, the magnitude of the deviatoric stress $\|\boldsymbol{\sigma}^*\|$ is kept constant. The numerical tests on a continuous principal stress axes rotation of 2α = 0 to 360° from the stress state R-1 and R-2 in Figure 1(b) are conducted. Figure 3 shows strain path induced during the imposed stress path under a pure principal stress axes rotation. The numerical result from R-1 exhibits a circular locus, and thus the strain components diminish at the end of a pure rotation of principal stress axes.

The result from R-2 brings about a larger circle and

an inelastic strain at the end of a stress cycle, as is often observed in the experimental results[1)-3)]. From a theoretical point of view, a phenomenological description of the deformation behaviour of elastoplastic materials to pure principal stress axes rotation has been examined[12)-14)] by the elastoplastic constitutive mode based on subloading surface model, with both tangent effect and anisotropy due to the rotation of the yield surface.

3. Phenomenological description of elastoplastic material responses

The phenomenological description of the deformation behaviour of soils to pure principal stress axes rotation is considered by the elastoplastic constitutive mode based on subloading surface model, with both tangent effect and anisotropy due to the rotation of the yield surface.

3.1 Non-coaxiality

The stretching $\mathbf{D}$ ($=(\mathbf{L}+\mathbf{L}^{\mathrm{T}})/2$) is additively decomposed into the elastic stretching $\mathbf{D}^e$ and the inelastic stretching $\mathbf{D}^i$, i.e.

$$\mathbf{D}=\mathbf{D}^e+\mathbf{D}^i \tag{9}$$

Further, let the inelastic stretching $\mathbf{D}^i$ be additively decomposed into plastic stretching $\mathbf{D}^p$ and tangential stretching $\mathbf{D}^t$, i.e.

$$\mathbf{D}^i=\mathbf{D}^p+\mathbf{D}^t \tag{10}$$

on the premise that $\mathbf{D}^p$ and $\mathbf{D}^t$ are induced by the stress-rate component normal and tangential, respectively, to the yield/loading surface in order to extend the traditional elastoplasticity so as to describe the general non-proportional loading behavior.

The plastic stretching $\mathbf{D}^p$ based on the consistency condition and the plastic potential is generally described as

$$\mathbf{D}^p=\frac{1}{M^p}\mathrm{tr}\left(\frac{\partial f}{\partial\boldsymbol{\sigma}}\overset{\circ}{\boldsymbol{\sigma}}\right)\frac{\partial g}{\partial\boldsymbol{\sigma}} \tag{11}$$

where f and g are the yield and the plastic potential function, respectively, and M^p is the plastic modulus, functions of stress and internal variables in general. The plastic constitutive equation (11) has the following properties:

(1) The plastic stretching $\mathbf{D}^p$ is independent of the stress-rate component tangential to the yield surface, called the tangential-stress rate, and its direction is independent of the stress rate. Needless to say, the plastic stretching is not induced in the stress path $(\mathrm{tr}\{(\partial f/\partial\boldsymbol{\sigma})\overset{\circ}{\boldsymbol{\sigma}}\}=0)$ tangential to the yield surface.

(2) An isotropic function of the stress tensor obeying the orthogonal transformation can be described by a function of principal stresses or invariants of stress. Then, if the yield function f is an isotropic function of the stress tensor leading to mechanically-isotropic yielding behavior, plastic stretching is not induced during the principal stress axes rotation process with constant values of the principal stresses.

(3) The coaxiality, i.e. the coincidence of the principal directions of plastic stretching with those of stress, holds as far as g is an isotropic function of the stress tensor. In fact, however, the non-coaxiality is observed in the experiments described for (2) and (3).

On the other hand, the inelastic stretching $\mathbf{D}^i$ given by Eq. (10) possesses the following properties.

(a) Not only the magnitude but also the direction of the inelastic stretching $\mathbf{D}^i$ exhibits a dependence on the stress rate.

(b) The non-coaxiality between inelastic stretching $\mathbf{D}^i$ and stress $\boldsymbol{\sigma}$ is caused by the existence of $\mathbf{D}^t$, even if an isotropic plastic potential surface of stress is adopted.

(c) The inelastic stretching induced during the rotation of the principal stress axes can be described by the incorporation of the tangent effect, even if an isotropic yield function of stress is used.

Here, consider the constitutive model with the anisotropic plastic potential surface, which exhibits non-coaxiality and in which the direction of the inelastic stretching depends only on the state variable but is independent of the rate variable. One should note the following facts:

(i) This model cannot describe the dependence of the inelastic stretching on the tangential stress-rate as long as the tangent effect is not incorporated. That is to say, the non-coaxial model without the tangent effect is incapable of predicting appropriately the stress probe behavior.

(ii) Further, the model cannot describe the inelastic stretching during the rotation of the principal stress axes as long as an anisotropic yield surface and/or the tangent effect is not incorporated. Inversely, inelastic stretching during the rotation of the principal stress axes is predicted even by the coaxial model with an isotropic plastic potential surface, only if an anisotropic yield surface is adopted.

3.2 Material functions

The concrete forms of material functions for soils are described in this section. The anisotropy of soils could be described concisely by the concept of the rotation of the yield surface around the origin of the stress space, called the rotational hardening by Hashiguchi (1977)[15)], originally proposed by Sekiguchi and Ohta (1977)[16)].

Let the loading function f be given for soils as

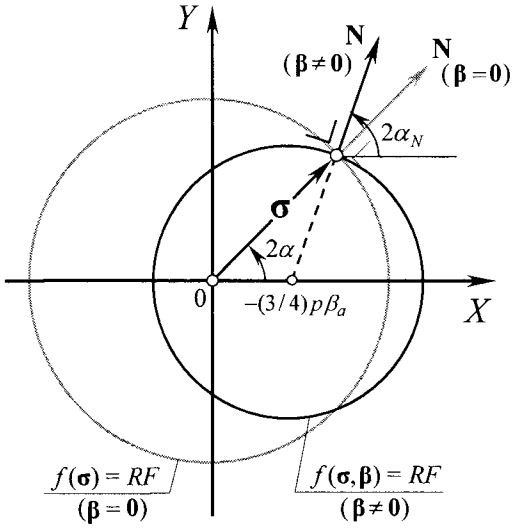

Figure 4 The subloading surfaces for isotropic ($\boldsymbol{\beta}=\mathbf{0}$) and anisotropic ($\boldsymbol{\beta}\neq\mathbf{0}$) soils illustrated in the (X, Y) plane.

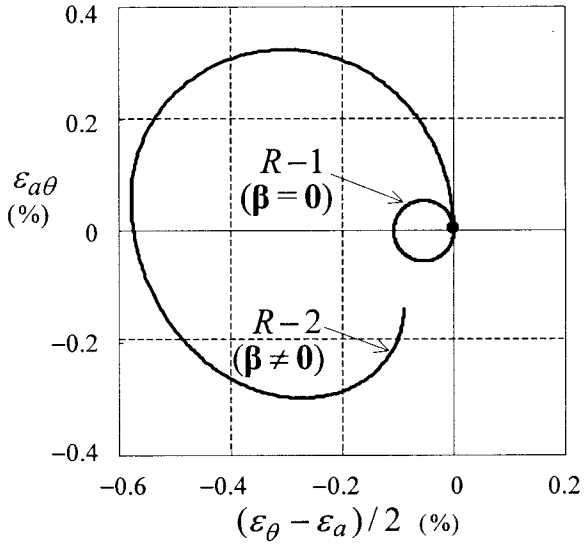

Figure 5 The inelastic strain in the principal stress rotation from the stress states *R*-1 and *R*-2.

$$f(\boldsymbol{\sigma},\mathbf{H}) = p(1+\chi^2) = F \tag{12}$$

where

$$p \equiv -\frac{1}{3}\mathrm{tr}\boldsymbol{\sigma}, \quad \chi \equiv \frac{\|\hat{\boldsymbol{\eta}}\|}{m}, \quad \hat{\boldsymbol{\eta}} \equiv \boldsymbol{\eta}-\boldsymbol{\beta} \tag{13}$$

$$\boldsymbol{\eta} \equiv \frac{\boldsymbol{\sigma}^*}{p}, \quad \boldsymbol{\sigma}^* \equiv \boldsymbol{\sigma} + p\mathbf{I} \tag{14}$$

In these equations, m is a material function of Lode's angle or the b-value and internal variables, representing the value of $\|\hat{\boldsymbol{\eta}}\|$ in the critical state, whilst the simplest function for m is given by Hashiguchi (2001)[17]. However, m is regarded as constant in this article since infinitesimal variations in the Lode's angle are considered. The scalar F is isotropic hardening/softening function. The tensor $\boldsymbol{\beta}$ is introduced to describe the anisotropy through the rotation of the yield surface around the origin of the stress space. For $\boldsymbol{\beta}=\mathbf{0}$ (isotropy), the meridian section of loading surface is half-ellipsoids whose long axes coincide with the hydrostatic axis in the stress space. Therefore, the function f in Eq. (12) is regarded as the extension of the modified Cam-clay model to the anisotropy due to the rotational hardening.

3.3 Loading surface in the (*X*, *Y*) stress plane

Anisotropy is often caused by the sedimentation of soil particles, which is also observed in sand samples made in laboratories, which is supported by the experimental fact that the bedding plane has the highest compression resistance but the lowest shear resistance due to the horizontal alignment of sub-elongated sand particles. Then, let the anisotropy for the axisymmetric condition be assumed as follows:

$$\boldsymbol{\beta} = \begin{bmatrix} -\beta_a/2 & 0 & 0 \\ 0 & -\beta_a/2 & 0 \\ 0 & 0 & \beta_a \end{bmatrix} \quad (\mathrm{tr}\boldsymbol{\beta}=0) \tag{15}$$

The rotation angle θ_β of the central axis of the yield surface in the (p, q_r) plane is given as follows:

$$\theta_\beta = \tan^{-1}(-\sqrt{\frac{3}{2}}\beta_a) \tag{16}$$

Substituting Eq. (15) into Eq. (12) leads to the following expression of the loading surface in terms of (X, Y) as

$$(X+\frac{3}{4}p\beta_a)^2 + Y^2 = \frac{1}{2}m^2(\frac{F}{p}-1) - \frac{3}{16}\beta_a^2 \tag{17}$$

The outward-normal vector $\mathbf{N}=(N_X, N_Y)$ of the loading surface in the (X, Y) stress plane is given as follows:

$$\left.\begin{matrix} N_X \\ N_Y \end{matrix}\right\} = \frac{1}{\sqrt{(X+\frac{3}{4}p\beta_a)^2+Y^2}} \left\{\begin{matrix} X+\frac{3}{4}p\beta_a, \\ Y. \end{matrix}\right. \tag{18}$$

The loading surfaces for the isotropy ($\boldsymbol{\beta}=\mathbf{0}$) and anisotropy ($\boldsymbol{\beta}\neq\mathbf{0}$) are shown in the (X, Y) stress plane (see. Fig. 4). The loading surface shifts to the X-axis direction with an increase in magnitude of the anisotropic parameter β_a. For isotropic conditions, the direction of the outward-normal vector $\mathbf{N}$ on the loading surface coincides with that of the stress in this plane. Therefore, the principal directions of the plastic stretching coincide

with those of the stress leading to coaxiality. On the other hand, for anisotropic conditions, the direction of the outward-normal vector **N** on the loading surface does not coincide with the direction of the stress in the plane, except for the case where $\sigma_{a\theta}$ =0. The angle $2\alpha_N$ of the direction of the outward-normal of the yield surface in the (X, Y) plane measured from the X-axis in the (X, Y) plane is given by Eq. (18) as

$$\tan 2\alpha_N = \frac{Y}{X + \frac{3}{4} p\beta_a} \tag{19}$$

It holds for α and α_N from Eqs. (17) and (18) that

$$\tan 2\alpha_N = \frac{\tan 2\alpha}{1 + \frac{3}{4}\frac{p}{\sqrt{X^2+Y^2}}\sqrt{1+\tan^2 2\alpha}\,\beta_a} \tag{20}$$

3.4 Deformation behaviour predicted by a phenomenological elastoplasticity model

The strain paths predicted by the phenomenological elastoplasticity models[13), 14)] is shown in Fig. 5 for R-1 and R-2 tests, keeping $\sqrt{X^2+Y^2}$ =21.2 kPa and =50 kPa at p=100 kPa, respectively, in which the following material constants and initial values are used in the calculation.

E = 310 MPa, ν = 0.2, ρ = 0.034, γ = 0.0034,
F_0 =350 kPa, m =0.96, β_a = −0.15, u =10,
a = 0.01, b = c = 1.0.

The prediction on R-1 test is conducted by the subloading surface model with the non-coaxiality induced only by the tangent effect, which exhibits a completely circular locus, and thus diminishes at the end of a stress cycle as shown in the calculation results in Fig 3. The prediction on R-2 test is conducted by the model with the non-coaxiality induced by both the tangent effect and anisotropy, which dose not exhibit perfectly circular locus, and thus dose not diminishes at the end of a stress cycle as shown in the calculation results in Fig 3 for R-2 test.

4. Concluding remarks

The macroscopic constitutive response of granular media to principal stress axes rotation has been examined in this study. The mechanical response of the granular element model to the non-proportional loading exhibits the following characteristics:

i) For the pure principal stress rotation, inelastic strain is not induced for the stress state close to isotropy (R-1 test).

ii) Inelastic strain is induced with increase in magnitude of the deviatoric stress (R-2 test).

In addition, the phenomenological description of the deformation behavior of soils is discussed from the view point of the non-coaxiality by adopting the subloading surface model with both the tangent effect and anisotropy due to the rotation of the yield surface. The mechanical response of the model for the principal stress axes rotation exhibits the following feature. Even during the pure principal stress axes rotation process where the principal stress value is kept constant, a rather large strain is induced, depicting an almost circular strain path in the deviatoric strain plane (it does not diminish), leaving an irreversible strain at the end of the stress cycle. It is verified that the present model has the capability of describing the non-proportional loading behavior of sands under the pure principal stress axes rotation. Eventually, it can be concluded that both the tangent effect and the anisotropy in the yield condition have to be incorporated into constitutive equations for the description of the general non-proportional loading behavior of soils.

REFERENCES

1) Miura, K., Miura, S. and Toki, S., Deformation behavior of anisotropic dense sand under principal stress axes rotation, Soils and Found., Vol. 26, No. 1, pp. 36-52, 1986.
2) Pradel, D., Ishihara, K. and Gutierrez, M., Yielding and flow of sand under principal stress axes rotation, Soils and Found., Vol. 30, No. 1, pp. 87-99, 1990.
3) Gutierrez, M., Ishihara, K. and Towhata, I., Flow theory for sand during rotation of principal stress direction, Soils and Found., Vol. 31, No. 4, pp. 121-132, 1991.
4) Cundall, P.A., Strack, O.D.L., A discrete numerical model for granular assemblies, Geotechnique, Vol. 29, pp. 47-65, 1979.
5) Kishino, Y., Computer analysis of dissipation mechanism in granular media, Powders and Grains, Rotterdam, A.A. Balkema, pp. 323-330, 1989.
6) Kishino, Y., The incremental nonlinearity observed in numerical tests of granular media, CD-ROM Proc. 15th ASCE Eng. Mech. Conf., 2002.
7) Wren, J.R. and Borja, R.I., Micromechanics of granular media, Part II: Overall tangential moduli and localization model for periodic assemblies of circular disks, Comput. Meth. Appl. Mech. Engrg., Vol. 141, pp. 221-246, 1997.
8) Kuhn, M.R., Structured deformation in granular materials. Mech. Mater., Vol. 31, pp. 407-429, 1999.
9) Goddard, J.D., On entropy estimates of contact forces in static granular assemblies, Int. J. Solids and Structures, Vol. 41, pp. 5851-5861, 2004.
10)Kaneko, K., Doctor Thesis, Tohoku University, 2001.
11)Kaneko, K., Terada, K., Kyoya, T. and Kishino, Y., Global–local analysis of granular media in quasi-static equilibrium, Int. J. Solids and Structures, Vol. 40, pp. 4043-4069, 2003.
12)Hashiguchi, K. and Tsutsumi, S., Elastoplastic constitutive

equation with tangential stress rate effect, Int. J. Plasticity, Vol.17, No. 1, pp. 117-145, 2001.

13)Tsutsumi, S., Hashiguchi, K., Okayasu, T., Saitoh, K. and Sugimoto, M., Mechanical response of the subloading surface model with tangential stretching, Journal of Applied Mechanics, JSCE, Vol. 4, pp. 375-382, 2001.

14)Tsutsumi, S. and Hashiguchi, K., General non-proportional loading behaviour of soils, Int. J. Plasticity, Vol. 21, No. 10, pp. 1941-1969, 2005.

15)Hashiguchi, K., An expression of anisotropy in plastic constitutive equations of soils, Constitutive Equations of Soils (Proc. 9th ICSMFE, Specialty Session 9), Tokyo, JSSMFE, pp. 302-305, 1977.

16)Sekiguchi, H. and Ohta, H., Induced anisotropy and time dependency in clays, Constitutive Equations of Soils (Proc. Spec. Session 9, 9th ICSMFE), Tokyo, pp. 229-239, 1977.

17)Hashiguchi, K., Description of inherent/induced anisotropy of soils: rotational hardening rule with objectivity, Soils and Found., Vol. 41, No. 6, pp. 139-145, 2001.

(Received April 15, 2005)